Oxygen reduction reaction mechanism on a phosporus-doped pyrolyzed graphitic Fe/N/C catalyst

by Febdian Rusydi

NJC

PAPER

View Article Online
View Journal | View Issue

Cite this: *New J. Chem.*, 2019, **43**, 11408

Oxygen reduction reaction mechanism on a phosporus-doped pyrolyzed graphitic Fe/N/C catalyst†

Hermawan K. Dipojono,*[ab] Adhitya G. Saputro,*[ab] Apresio K. Fajrial,[c] Mohammad K. Agusta,[ab] Fiki T. Akbar,[d] Febdian Rusydi[ef] and Dedy H. B. Wicaksono[g]

Received 25th April 2019,
Accepted 25th June 2019

DOI: 10.1039/c9nj02118c

rsc.li/njc

The oxygen reduction reaction (ORR) mechanism on the active sites of a phosphorus-doped pyrolyzed Fe/N/C catalyst is examined by using density functional theory based calculations. The introduction of the phosphorus dopant creates three initial possible active sites for the ORR *i.e.*, FeN_4, C–N and P-doped sites. In the presence of O_2, the P-doped sites become passivated while the rest of the catalyst sites are still functional. The ORR profile for the associative mechanism (the O_2 molecule is reduced from its molecular form) on the FeN_4 site is practically unaffected by the presence of the neighboring P=O site. However, the ORR profile for the dissociative mechanism (the O_2 molecule is reduced from its dissociated form) on the FeN_4 site is significantly improved as compared to that on the undoped Fe/N/C catalyst system. This phenomenon is mainly induced by the distortion of C–C networks due to the presence of the neighboring FeN_4 and P=O sites, which leads to the stabilization of the *OH adsorption state on the C atoms next to the FeN_4 site.

1 Introduction

In recent years, non-precious metal catalysts (NPMCs) have drawn huge attention due to their appealing performance for the oxygen reduction reaction (ORR).[1,2] The development of NPMCs is motivated by the quest for alternative catalysts to replace scarce and costly platinum-based (Pt) materials as the cathode catalyst in hydrogen fuel cells. Pyrolyzed Fe/N/C is a type of NPMC which is fabricated by applying high temperature pyrolysis to iron/nitrogen/carbon containing moieties. Among many type of NPMCs, the pyrolzyed Fe/N/C catalyst has a promising ORR activity and high stability under fuel cell working conditions.[1,2] However, the overall performance of this catalyst has not overpowered the current state-of-the-art Pt catalyst.[3–5] Therefore, further study to improve the pyrolyzed Fe/N/C catalyst performance is very important.

Pyrolyzed Fe/N/C is a heterogeneous catalyst that consists of several types of iron–nitrogen complex (Fe–N_x) and metal-free active sites.[6–8] This fact raises several intensive discussions regarding the origin of the high catalytic activity of pyrolyzed Fe/N/C.[9–11] In addition, due to its heterogeneous nature, these active sites might be formed next to each other in the real sample. Various theoretical studies have been reported on the O_2 molecule interaction and ORR mechanism on the stand alone transition metal–nitrogen complex (TM–N_x)[12–25] or metal-free active sites.[26–39] Nonetheless, the interaction between neighboring active sites is always ignored. Our recent studies demonstrated that the interaction between neighboring active sites is actually very beneficial since it can increase their stability and the local ORR activities. We demonstrated that the interaction of the FeN_4 and quaternary-N sites at the zigzag edge of graphene could significantly improve the free energy profile for the ORR on the C atoms next to the quaternary-N site.[40] We also studied the effect of adding boron doping (B) to the pyrolyzed Fe/N/C system.[41] The formation of the neighboring FeN_4 and B–N sites not only increases the stability but also enhances the interaction between the FeN_4 site and an O_2 molecule.

[a] Research Center for Nanosciences and Nanotechnology, Institut Teknologi Bandung, Jl. Ganesha 10, Bandung 40132, Indonesia. E-mail: dipojono@tf.itb.ac.id, ganda@tf.itb.ac.id
[b] Advanced Functional Materials Research Group, Institut Teknologi Bandung, Jl. Ganesha 10, Bandung 40132, Indonesia
[c] Department of Mechanical Engineering, University of Colorado, Boulder, CO 80309, USA
[d] Theoretical High Energy Physics and Instrumentations Research Group, Institut Teknologi Bandung, Jl. Ganesha 10, Bandung 40132, Indonesia
[e] Theoretical Physics Research Group, Department of Physics, Faculty of Science and Technology, Airlangga University, Surabaya 60115, Indonesia
[f] Research Center for Quantum Engineering Design, Airlangga University, Surabaya 60115, Indonesia
[g] Department of Biomedical Engineering, Faculty of Life Sciences and Technology, Swiss German University, Tangerang 15143, Indonesia

† Electronic supplementary information (ESI) available. See DOI: 10.1039/c9nj02118c

The presence of these neighboring active sites allows the incoming O_2 molecule to be adsorbed with a side-on bridging configuration on top of the Fe and B atoms and this results in a facile O_2 dissociation process. Holby *et al.* also showed a similar trend for the O_2 interaction with the Fe–Fe atoms of neighboring FeN_x sites.[42] Obviously, these kind of interactions cannot occur in a single FeN_4 site system. All of these studies encourage, theoretically, a new strategy that might be used to improve the ORR activity of the pyrolyzed Fe/N/C-type catalyst by forming closely neighboring FeN_x and/or metal-free active sites.

Recently, catalysts made of phosphorous-doped (PG) or dual phosphorous–nitrogen-doped graphene (PNG) with various active site configurations have been reported to interact well with O_2 molecules and exhibit good ORR performance.[43–58] All of the reported active sites for PG and PNG systems maintain their graphitic structure, even though there are some distortions caused by the large atomic radii of the P atom. Inspired by the success of PG and PNG catalysts, Hu *et al.* tried to improve the ORR activity of the standard pyrolyzed Fe/N/C catalyst by introducing P doping into the catalyst.[59] They find that this catalyst has a similar onset potential to the standard pyrolyzed Fe/N/C catalyst but it has much higher current densities in the mixed kinetic and diffusion limited regions. However, the origin of this significant improvement is still unclear. The active sites of this catalyst are believed to be not significantly altered from the original active site configurations of the Fe/N/C and PNG catalysts. Therefore, the activity improvement of this catalyst might originate from the interaction of the active sites of the Fe/N/C and the PNG systems.

In this work, we study the interaction between FeN_4 and metal-free sites of the P-doped pyrolyzed Fe/N/C catalyst and its effect on their local ORR free energy profiles using density functional theory-based calculations. Since the pyrolyzed Fe/N/C catalyst has a similar graphitic structure to the P-doped graphene system, the original active site configurations can be retained in the P-doped pyrolyzed Fe/N/C system and might be formed neighboring each other. ORR mechanisms and possible thermodynamic rate-determining steps on these active sites are studied by inspecting their free energy profiles.

2 Computational details

We use one layer of a graphene 6 × 6 sheet with an embedded FeN_4 site as the model of the catalyst active site. It has been experimentally confirmed that the activity of the graphene system embedded with FeN_x is independent of the number of graphene layers.[60] Therefore, one layer of graphene is appropriate to model the active site structure. We choose FeN_4 to represent the FeN_x sites of the pyrolyzed Fe/N/C catalyst since this site is the most stable FeN_x configuration and active toward O_2 molecules.[23,61,62] The metal-free active site is represented by a pair of N–P atoms substituting two C atoms in the unit cell. The configuration that we used for this study is the simplest model since we only consider one N atom as the metal-free site, and one P atom as the dopant. The model of this active site configuration is relevant to the experiment of Hu *et al.*[59] They show that the XPS profiles of P doped Fe/N/C active sites are very similar to the standard Fe/N/C and PNG catalysts. Hence, significant modifications in the structure of the active sites of the P doped Fe/N/C catalyst are not expected.

The most stable P–N pair configuration in the graphene system embedded with FeN_4 (FeN_4G-NP) is determined using two steps of substitutional atom addition.[41] The first step is done by locating one substitutional atom (either N or P) which yields the lowest total energy. From our previous study, we find that the location of the N substitutional site (N_{subs}) is almost independent of the FeN_4 site since the variation of the total energy with respect to the N_{subs}–FeN_4 distance is negligible (except when the location of the N_{subs} site is next to the N atom of the FeN_4 site the total energy of the system increases significantly).[41,63] Therefore, to obtain the most stable FeN_4G-NP configuration we only need to look at the most stable location of the P substitutional site (P_{subs}) first and then find the second substitutional site (N site) which gives the lowest total energy for the system.

Spin-polarized density functional theory[64,65] calculations are performed using the Quantum-Espresso package version 5.4.[66] Exchange and correlation effects are incorporated within the generalized gradient approximation, using the Perdew–Burke–Ernzerhof (PBE) functional.[67] Kohn–Sham eigenfuctions are expanded in plane-wave basis sets where the interactions between valence electrons and ion cores are described by ultrasoft pseudopotentials[68] taken from the Quantum-Espresso database. Converged results are achieved by using cutoff energies of 30 Ry for the plane wave and of 360 Ry for the electronic density. The effect of van der Waals interactions is described by using the semi-empirical correction scheme of Grimme, DFT-D2.[69] The Brillouin zone sampling for all systems, except isolated molecules, is performed with a 2 × 2 × 1 k-point mesh for the structural and electronic properties. Calculations for isolated molecule are done at the gamma point in a 30 × 30 × 30 Å^3 cubic cell. All of the systems are fully relaxed until the residual force on each atomic component is less than 0.025 eV Å^{-1}. The vibrational frequencies of adsorbed molecules are calculated to obtain the zero-point energy contribution in the free energy expression. In this calculation, only adsorbate vibrational modes are calculated explicitly, while the surface modes are fixed. Vibrational frequencies are computed by displacing each atom of the adsorbate by 0.01 Å in each of three cartesian directions and by diagonalizing the resulting Hessian matrix. Forces of the displaced adsorbate are calculated by the Quantum-Espresso package while the diagonalization step is performed in the Atomistic Simulation Environment (ASE).[70] Saddle points of some reactions are calculated by the climbing image nudged elastic band method (CI-NEB).[71]

The adsorption energy of a molecule on a surface is defined as:

$$E_{ad} = E_{tot} - (E_{surf} + E_{molecule}) + \Delta ZPE, \quad (1)$$

where E_{tot} corresponds to the total energy of the combined system, E_{surf} corresponds to the total energy of the clean surface, $E_{molecule}$ corresponds to the total energy of the isolated

molecule and ΔZPE corresponds to the change in zero point energy corrections.

To calculate the change in free energy of a reaction that involves an electron transfer step, we follow the approximation in ref. 72. Briefly, the chemical potential of $[H^+ + e^-]$ under standard conditions (pH = 0, p = 1 bar, T = 298.15 K, and electrode potential U = 0 V) is related to the chemical potential of 1/2 H_2 by using the standard hydrogen electrode. The change in free energy (ΔG) of reaction $A + H^+ + e^-(U) \rightarrow AH$ is calculated using the following equation:

$$\Delta G(U) = G(AH) - G(A) - \frac{1}{2}G(H_2) - pHk_BT\ln 10 + eU, \quad (2)$$

where G(X) is the Gibbs free energy of compound X (eV) and k_B is the Boltzmann constant. This equation could be expressed as:

$$\Delta G(U) = \Delta G_0 + eU, \quad (3)$$

where ΔG_0 is the change in free energy at electrode potential U = 0 V (short circuit condition). From this, we can see that the relation between the change in free energy and the electrode potential U within this approximation is linear. Since we are interested in the reaction in an acidic medium, we assumed that pH = 0. We also neglect the contribution from an electrochemical double layer.[72]

The overpotential of a catalyst (η) in this approximation is defined as $\eta = U^0 - U^{onset} = \Delta G_{max}(U^0)/e$.[72] U^0 represents the equilibrium potential or maximum cell voltage, which is 1.23 V. U^{onset} represents the maximum electrode potential value which makes a particular reaction pathway start to have an uphill profile (endothermic). $\Delta G_{max}(U^0)$ represents the maximum ΔG value at U = 1.23 V for a reaction in a particular reaction pathway. The thermodynamic rate-determining step (RDS) for a reaction pathway can be determined by finding a step which gives either U^{onset} or $\Delta G_{max}(U^0)$ since these quantities are linearly dependent.

3 Results and discussion

3.1 The structure of FeN_4G-NP

The relative energies and the location of the five most stable P_{subs} sites are shown in Table 1 and Fig. 1a and b. Due to its larger atomic radius, the substitution of a C atom with a P atom distorts the local planarity of the FeN_4G structure (for example see Fig. 1b). Our results suggest that the stability of the system decreases as the P_{subs}–FeN_4 distance increases. In its most stable P–FeN_4G configuration (P1), the substitutional P atom

Table 1 Five P_{subs} configurations with the lowest relative energies as indicated by the distance (Å) between P_{subs} and the center of the FeN_4 site

P_{subs} site	P_{subs}–FeN_4 (Å)	Relative energy (eV)
P1	3.168	0.00
P2	3.561	0.17
P3	2.852	0.30
P4	4.876	0.79
P5	4.876	0.85

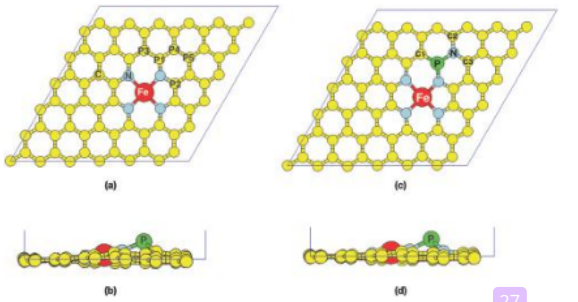

Fig. 1 (a) Location of the five most stable P_{subs} sites. (b) Side view geometry of the most stable P_{subs} site configuration. (c) Top-view and (d) side-view of the most stable configuration of the FeN_4G-NP system.

prefers to form a direct bond with the N atom of the FeN_4 site as shown in Fig. 1a.

The N_{subs} atom is introduced into the FeN_4G-P system to form the FeN_4G-NP configuration. The location of N_{subs} sites is varied and their energies are compared while keeping the position of the $P1_{subs}$ site. The most stable FeN_4G-NP configuration is shown in Fig. 1c and d. The structures and relative energies of less stable configurations of the other P–N pairs are shown in Fig. S1 of the ESI.† In the most stable configuration, both P_{subs} and N_{subs} atoms bond to each other and form a N_{subs}–P_{subs}–N link with the N atom of the FeN_4 site. This situation is very similar to the case of the boron (B) doped case in the FeN_4G-NB system[41] since B and P have similar electronegativity. The origin of this phenomenon is due to the nature of N as an electron acceptor and P as an electron donor. The P–N interaction neutralizes their presence, thereby preserving the stability of the system.

We calculate and compare the formation energies of the FeN_4G-NP configuration with the other active site configurations of the pyrolyzed Fe/N/C catalyst (*i.e.*, undoped FeN_4G,[13,61,73,74] P-doped graphene (PG),[45,50] N-doped graphene (NG),[75–77] and PN co-doped graphene (PNG)[47]) to understand their relative stabilities. We approximate the relative formation energies of these structures based on their total energies following ref. 78 and 79 using the following equation:

$$E_{Formation} = E_{Structure} - (n_C\mu_C + n_{Fe}\mu_{Fe} + n_N\mu_N + n_P\mu_P + n_O\mu_O). \quad (4)$$

The negative value of $E_{Formation}$ indicates that the corresponding structure might be formed spontaneously. The value of $E_{Structure}$ corresponds to the total energy of the active site structure. The values of n_C, n_{Fe}, n_N, n_P and n_O correspond to the number of C atoms, Fe atoms, N atoms, P atoms and O atoms in the unit cell.‡ μ_C, μ_{Fe}, μ_N, μ_O and μ_P correspond to the chemical potential values of the C atom, Fe atom, N atom, P atom and O atom, respectively. The values of μ_C, μ_{Fe} and μ_O are defined as the energy per C atom in pristine graphene, the energy per Fe atom in bcc bulk phase iron and the energy per O atom in an O_2 molecule, respectively. The values of μ_N and μ_P

‡ The presence of an O atom will be used to discuss the formation of FeN_4G-NP=O in the next subsection.

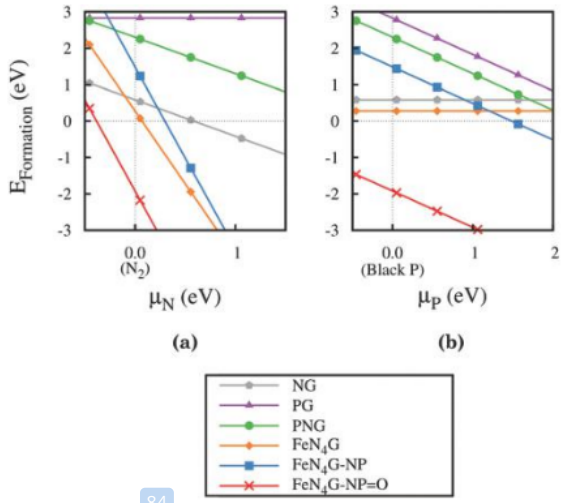

Fig. 2 Plot of the formation energy of the active site configurations as a function of (a) μ_N and (b) μ_P.

are assumed to be tunable during experiments.[80] For reference purposes, the zero for μ_N is taken from the energy per N atom in a N_2 molecule while the zero for μ_P is taken from the energy per P atom in a bulk phase of black phosphorus.[81–83]

The results of the calculations of the formation energy as a function of μ_N and μ_P are shown in Fig. 2. According to the figure, the FeN_4G-NP configuration has an exothermic profile (negative formation energy) starting at a low μ_N value, comparable to the conventional FeN_4G active site configuration. On the other hand, the exothermic profile for this configuration arises at quite a high μ_P value, similar to the profiles of its well known metal-free versions, which are the PG[45,50] and PNG[47] configurations. However, we should also notice from the diagram that the formation energy of the FeN_4G-NP configuration is actually much lower than that of the PG and PNG configurations, indicating that the FeN_4G-NP configuration can be formed with a higher probability. In the next subsection, we will show that the relative stability of this FeN_4G-NP configuration actually can be further improved by introducing oxygen into the system to form the FeN_4G-NP=O configuration.

3.2 O_2 adsorption on FeN_4G-NP

O_2 adsorption is one of the most important steps in the ORR process. The reduction of oxygen cannot occur without proper O_2 adsorption on the catalyst. Therefore, we begin our discussion of the ORR on the FeN_4G-NP system with the mechanism of O_2 adsorption.

Important results for the O_2 adsorption on the active site of the FeN_4G-NP system are presented in Table 2 and Fig. 3. We compare these results with the O_2 adsorption on the FeN_4 site of undoped FeN_4G and the C–N site of PN doped graphene (G-N_3PO). We specifically choose the G-N_3PO configuration to represent the active site configuration of PN doped graphene because this configuration is reported to give the lowest average ORR overpotential over various possible P–N doping configurations.[47] The data in Table 2 show that while the O_2 adsorption energies on the FeN_4 and C–N sites of the FeN_4G-NP system are slightly weaker, its O_2 adsorption configurations are rather similar to those on the FeN_4G and G-N_3PO systems. The distortion of the C–C networks around the P_{subs} site increases the total energy of the system and this contributes to the slight weakening of the O_2–FeN_4G-NP interaction. We also find an interesting feature in the case of O_2 adsorption on the FeN_4 site of the FeN_4G-NP configuration. The O–O bond elongation in this system is larger than that on undoped FeN_4G, even though its O_2 adsorption is weaker. This condition arises due to an additional interaction between a dangling bond on the P_{subs} site and the free O atom of the adsorbed O_2 molecule. This interaction occurs through the

Table 2 Important results for O_2 adsorption for various active site configurations. X represents the central atoms of the active sites, which are Fe, P and C atoms for FeN_4, P_{subs} and C–N sites, respectively

Configuration	Active site	X–O (Å)	X–O–O (°)	O–O (Å)	E_{ads} O_2 (eV)	Adsorption configuration
FeN_4G-NP	FeN_4	1.836	119.53	1.316	−0.87	End-on
	P_{subs}	1.713	58.42	1.568	−1.99	Side-on
	C–N	3.166	93.23	1.251	−0.15	End-on
FeN_4G-NP=O	FeN_4	1.745	121.51	1.293	−0.95	End-on
	C–N	3.187	93.23	1.241	−0.12	End-on
FeN_4G	FeN_4	1.808	119.99	1.297	−0.96	End-on
G-N_3PO	C–N	2.900	95.42	1.259	−0.23	End-on

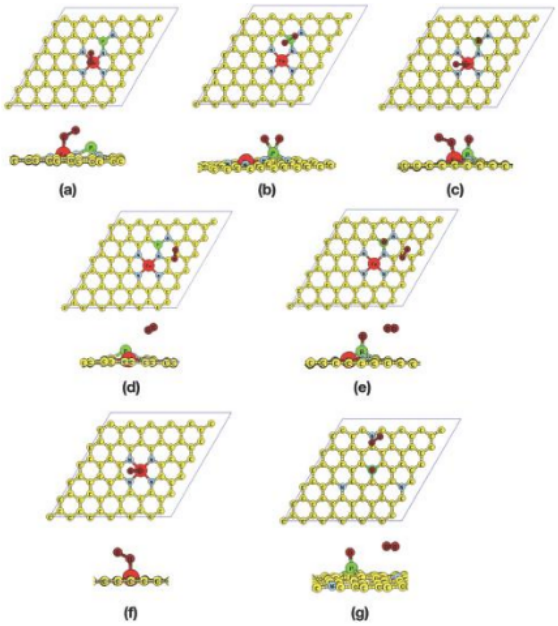

Fig. 3 Top and side views of O_2 adsorption on: (a) the FeN_4 site of FeN_4G-NP, (b) the P_{subs} site of FeN_4G-NP, (c) the FeN_4 site of FeN_4G-NP=O, (d) the C–N site of FeN_4G-NP, (e) the C–N site of FeN_4G-NP=O, (f) the FeN_4 site of undoped FeN_4G and (g) the C–N site of GN_3PO.

formation of an additional bonding state between the localized p_z orbital of the P atom and $2\pi^*$ orbitals of the adsorbed O_2 molecule (located right below the Fermi level, see Fig. S3 and S4 of the ESI†). The occupation of this state enhances the repulsion between the O atoms of the adsorbed O_2 molecule and results in the extra elongation of the O–O bond. This kind of mechanism is absent for the case of O_2 adsorption on the undoped FeN_4G configuration.

We also investigate the adsorption of an O_2 molecule on top of the P_{subs} site. We find that the O_2 molecule is adsorbed on this site with side-on adsorption and a very large O–O bond elongation (see Fig. 3b), similar to the case of O_2 adsorption on P doped graphene.[50] Evidently, from Table 2 we can see that this configuration is the most stable O_2 adsorption configuration on the FeN_4G-NP system, with an adsorption strength twice of that on the FeN_4 site. This finding suggests that the incoming O_2 molecule will likely approach the P_{subs} site with higher probability than the other two adsorption sites. The formation of O_2 side-on adsorption on the P_{subs} site arises from the interactions of the localized p_z state of the P atom and the bonding orbitals of the O_2 molecule (2π and 2σ). The bonding states resulting from these interactions are shown in Fig. S5 of the ESI.†

We perform an O_2 dissociation calculation on the P_{subs} site to check the stability of the adsorbed O_2 since its O–O bond is highly elongated. In the final state, we find that one of the O atoms of the adsorbed O_2 molecule stays at the P_{subs} site and the other one prefers to move to the top of the Fe atom of the FeN_4 site (2O–FeN_4-NP configuration). Our calculation shows that this dissociation reaction is actually a barrierless process. This result suggests that an incoming O_2 molecule approaching the P_{subs} site of the FeN_4-NP system will not stay adsorbed on the P atom in its molecular form, instead it will spontaneously dissociate and directly form a 2O–FeN_4-NP configuration.

We also calculate the energies required for removing one O atom from the 2O–FeN_4-NP configuration to estimate the stability of the adsorbed O atom on the FeN_4 site and P_{subs} site. The energies required for removing one O atom from the FeN_4 site and P site in the 2O–FeN_4-NP configuration are found to be −1.13 eV and −3.30 eV, respectively. As we will discuss in the next subsection, the adsorbed O atom on the FeN_4 site can be reduced easily into water due to its weaker adsorption strength. However, this is not the case for the adsorbed O atom on the P_{subs} site. The formation of the P═O configuration stabilizes the localized p_z state of the P_{subs} site (through the $p_z^P + p_z^O$ interaction) away from the Fermi level as indicated in Fig. S6 of the ESI.† This interaction makes the P═O bond become very strong and difficult to dissociate ($E_{ad}^O \sim -3.30$ eV). Moreover, our calculation shows that the reduction of *O on the P_{subs} site into *OH has a very endothermic profile even at $U = 0$ V ($\Delta G = 0.95$ eV), indicating a difficult reduction process. Hence, the first reduction step will prefer the complete reduction of *O on the FeN_4 site into water over the reduction of *O on the P_{subs} site. This reaction will leave us only with a very stable O atom adsorbed on the P_{subs} site of the FeN_4-NP configuration. If the subsequent reaction ought to proceed, it will be a competition between two possible reactions: (1) reduction of the P═O configuration into P–OH or (2) O_2 adsorption on the empty FeN_4 site. The system will most likely prefer the O_2 adsorption since this is not an activated process, as compared to the reduction of the P–O configuration. Therefore, the P═O configuration can be considered as a stable configuration acknowledging the strong adsorption of the O atom on the P_{subs} site. This configuration is referred to as the FeN_4G-NP═O configuration. A simplified schematic of the formation of this FeN_4G-NP═O configuration is shown in Fig. 4.

We calculate the formation energy for the FeN_4G-NP═O configuration to see the effect of the adsorbed O atom on the P_{subs} site. We observe that the termination of the dangling bond on the P_{subs} site by forming a P═O bond stabilizes the system. This result is shown in Fig. 2. We can see that the FeN_4G-NP═O configuration already has an exothermic profile even at very low μ_N and μ_P values. This finding also suggests that the FeN_4G-NP═O configuration can be formed easily with a higher probability as compared to the other active site configurations if an O_2 molecule is involved in the formation process. The formation of the graphitic P–O structure is in line with the appearance of P–C and P–O peaks in the P 2p XPS spectra of the P doped Fe/N/C catalyst.[59,84] Therefore, from this point we will use the FeN_4G-NP═O configuration as the main active site structure for the ORR process.

We calculate the O_2 adsorption on the possible active sites of the FeN_4G-NP═O configuration. Initially, there are three possible active sites for O_2 adsorption on the original FeN_4G-NP configuration as listed in Table 2. However, in the FeN_4G-NP═O configuration the P_{subs} site is not available for O_2 adsorption since it is passivated by an O atom. Therefore, only two possible sites are available for O_2 adsorption for this configuration: (1) the FeN_4 site and (2) the C atoms around the NP═O site. Results of O_2 adsorption on these sites are given in Table 2.

As in the case of the FeN_4G-NP configuration, we find that an O_2 molecule is strongly adsorbed on the FeN_4 site of the

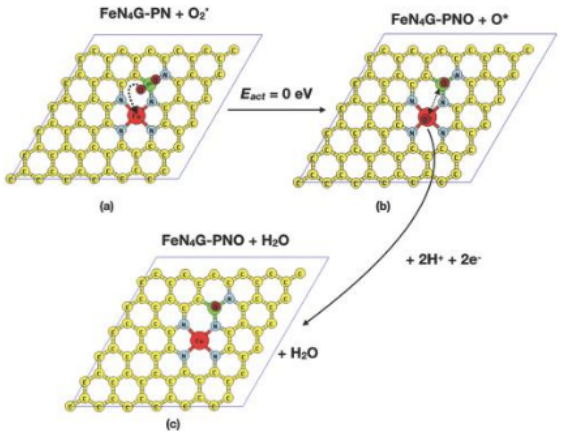

Fig. 4 A simplified schematic of the formation of the FeN_4G-NP═O configuration. (a) O_2 side-on adsorption on the P_{subs} site, (b) the dissociation of the adsorbed O_2 molecule and (c) the reduction of the adsorbed O atom on the FeN_4 site.

FeN_4G-NP═O configuration while it is only weakly physisorbed on the C–N site. However, the O–O bond elongation on the FeN_4 site of the FeN_4G-NP═O configuration is quite similar to that on the FeN_4 site of the undoped FeN_4G configuration. This is because, in contrast with the case of O_2 adsorption on the FeN_4G-NP configuration, the localized p_z state of the P_{subs} site of the FeN_4G-NP═O configuration cannot interfere with the adsorbed O_2 molecule on the FeN_4 site since it is already stabilized by the adsorbed O atom. In addition to this, due to steric hindrance, the free O atom of the adsorbed O_2 has to face the opposite direction to the P–O site. This adsorption configuration is shown in Fig. 3c. The O_2 adsorption energy and the end-on adsorption configuration on the FeN_4 site of FeN_4G-NP═O are very similar to the O_2 adsorption on typical FeN_4 active site configurations such as in FeN_4G,[13,14,22,23] Fe porphyrin[85,86] and Fe tape-porphyrin[87] systems.

For the case of adsorption on the C–N site, even though the O_2 molecule is only weakly physisorbed, the O_2 adsorption energy on the C–N site of the FeN_4G-NP═O configuration is slightly weaker than that of the G-N_3PO configuration. A theoretical study conducted by Gracia-Espino shows that P–N doped graphene works best towards the ORR only when the N_{subs} sites are not in direct contact with the P═O site, since this will bring the localized states of the C atoms around the N_{subs} and P═O toward the Fermi level, which will facilitate the C–O_2 interaction.[47] However, when the N_{subs} site is close to the P═O site, the localized states of the surrounding C atoms will be shifted far from the Fermi level and this will hinder the C–O_2 interaction. This mechanism explains why the O_2 molecule adsorption energy on the C–N site of the FeN_4G-NP═O configuration is weaker than that of the G-N_3PO configuration since the N_{subs} site of the FeN_4G-NP═O configuration is directly bonded to its P═O site. A comparison of the O_2 adsorption configuration on the C–N site of the FeN_4G-NP═O and G-N_3PO configurations is shown in Fig. 3e and g.

3.3 ORR mechanism on FeN_4G-NP═O

In this section we will only discuss the ORR mechanism on the FeN_4G-NP═O configuration since the P_{subs} site of the FeN_4G-NP configuration will always be poisoned by an O atom when an O_2 molecule interacts with this site. In the previous subsection, we find two stable O_2 adsorption configurations that exist on the FeN_4G-NP═O system: (1) strong end-on adsorption on the FeN_4 site and (2) weak physisorption on the C–N site. In general, there are two possible mechanisms for the ORR: associative and dissociative mechanisms. The main difference lies in the involvement of direct dissociation of the adsorbed O_2 molecule for the dissociative mechanism. The associative mechanism could happen on the FeN_4 and C–N sites. However, the dissociative mechanism could only happen on the FeN_4 site since no noticeable O–O elongation exists in the O_2 physisorption on the C–N site. We will also compare the ORR profiles for the related reduction mechanism on the FeN_4 site of the undoped FeN_4G system and the C–N site of the G-N_3PO system.

3.3.1 Associative mechanism. We calculate the ORR free energy profiles for the following reactions, which represent the associative mechanisms on the FeN_4 site of the FeN_4G and FeN_4G-NP═O systems and the C–N site of the G-N_3PO and FeN_4G-NP═O systems:

$$* + O_{2(g)} \rightarrow *O_2 \quad (5)$$

$$*O_2 + H^+ + e^-(U) \rightarrow *HO_2 \quad (6)$$

$$*HO_2 + H^+ + e^-(U) \rightarrow 2*OH \quad (7a)$$

$$*HO_2 + H^+ + e^-(U) \rightarrow *O + H_2O_{(l)} \quad (7b)$$

$$*HO_2 + H^+ + e^-(U) \rightarrow H_2O_2 + * \quad (7c)$$

$$2*OH + H^+ + e^-(U) \rightarrow *OH + H_2O_{(l)} \quad (8a)$$

$$*O + H^+ + e^-(U) \rightarrow *OH \quad (8b)$$

$$*OH + H^+ + e^-(U) \rightarrow H_2O_{(l)} + *, \quad (9)$$

where * represents an empty adsorption site and *X represents an adsorbed X species.

The direct four-electron reduction pathway to form water is composed of two main branches:

A (5) → (6) → (7a) → (8a) → (9)

B (5) → (6) → (7b) → (8b) → (9).

Reaction pathways A and B mainly differ in the formation of 2*OH (7b) and *O + H_2O (7a), respectively. We also calculate the ORR profiles for the possible two-electron reduction pathway to produce H_2O_2, which is represented by the following sequence:

C (5) → (6) → (7c).

The calculated ORR profiles for the associative mechanism on the FeN_4 and C–N sites at U = 0 V are shown in Fig. 5 and 6, respectively. The ORR profiles at equilibrium potential U = 1.23 V are presented in Section S4 of the ESI.†

For the case of the FeN_4 site, all of the reaction steps are found to have downhill profiles on both reaction pathways. We find that a H_2O_2 molecule cannot be formed on the FeN_4 site of the FeN_4G-NP═O system from the $*HO_2 + H^+ + e^-$ reaction since the adsorbed molecule will dissociate spontaneously into 2*OH or *O + H_2O. This situation is similar to the undoped

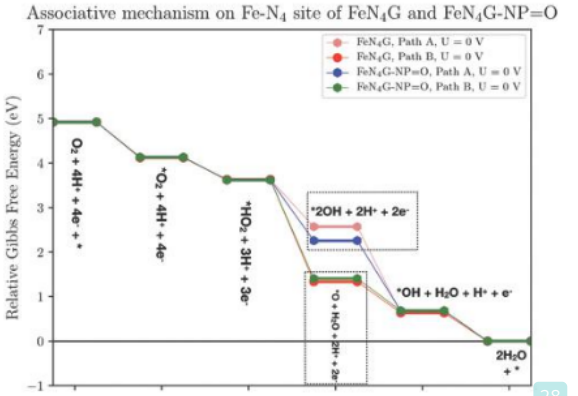

Fig. 5 ORR energy profiles for the associative mechanism on the FeN_4 site of the FeN_4G-NP═O system compared to that of the undoped FeN_4G system.

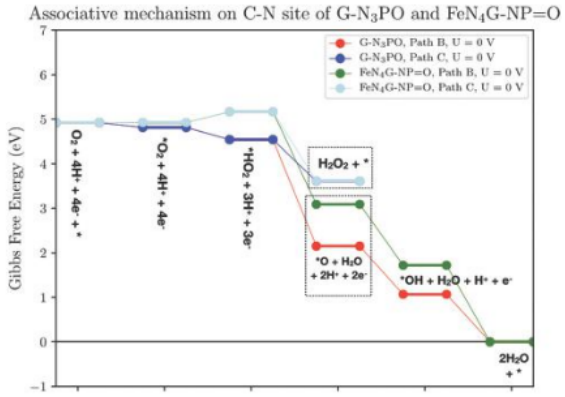

Fig. 6 ORR energy profiles for the associative mechanism on the C–N site of the FeN_4G-NP=O system compared to that of the G-N_3PO system.

FeN_4G system.[22,40] This result supports the experimental finding that shows a very low H_2O_2 yield on the P doped Fe/N/C catalyst.[59] On this catalyst, the H_2O_2 molecule can only be formed on the C–N and C–N–P=O active sites as we will demonstrate in the following paragraphs. From Fig. 5, we can see that the FeN_4G-NP=O system has a similar ORR profile to the undoped FeN_4G system since the energy plots almost coincide for all reaction steps, except for the 2*OH adsorption state. The 2*OH adsorption state on the FeN_4 site of the FeN_4G-NP=O system is more stable because the H atom from one of the formed *OH weakly interacts with the O atom of the P=O site (see Fig. S10 of the ESI†). This interaction makes the *OH adsorption state become more stable. Such an interaction is absent in the case of 2*OH adsorption on the undoped FeN_4G system.

The calculated onset potential (U^{onset}) and overpotential (η) for the associative mechanism through both reaction pathways on the FeN_4 site of the FeN_4G and FeN_4G-NP=O systems are tabulated in Table 3. U^{onset} for the FeN_4G and FeN_4G-NP=O systems is 0.49 V and 0.51 V, corresponding to η values of 0.74 V and 0.72 V, respectively. The thermodynamic RDS for the ORR on these systems can be determined by locating the reactions which give U^{onset}. The RDS for both systems is caused by reaction (6), which is $*O_2$ reduction to $*HO_2$. The FeN_4G-NP=O system has a better η value ($\sim$0.02 V) because the $*HO_2$ adsorption state on this system is more stable.

Table 3 Onset potential (U^{onset}), overpotential (η) and rate determining-step (RDS) for the ORR on selected active sites

System	Active site	ORR mechanism	Reaction pathway	U^{onset}(V)	η(V)	RDS
FeN_4G-PN=O	FeN_4	Associative	A	0.51	0.72	(6)
			B	0.51	0.72	(6)
		Dissociative	D	0.83	0.40	(14a)
			E	0.68	0.55	(15b)
	C–N	Associative	B	−0.24	1.47	(6)
			C	−0.24	1.47	(6)
FeN_4G	FeN_4	Associative	A	0.49	0.74	(6)
			B	0.49	0.74	(6)
		Dissociative	D	0.30	0.93	(14a)
			E	0.63	0.60	(15b)
G-N_3PO	C–N	Associative	B	0.27	0.96	(6)
			C	0.27	0.96	(6)

From the above discussions, the presence of the P=O site does not negatively affect the ORR profile of the FeN_4 site for the associative mechanism. Instead, we find some slight improvement in the ORR profiles of the FeN_4G-NP=O and undoped FeN_4G configurations. In general, the overpotential and RDS for the FeN_4 site of the FeN_4G-NP=O system still remain comparable with the FeN_4 site of the typical FeN_4G system.[23,40,88]

For the case of the associative mechanism on the C–N site of the FeN_4G-NP=O system, we find that only the first hydrogenation step to form HO_2 (reaction (6)) has an uphill profile while the rest of the reactions have downhill profiles at U = 0 V. This is very different from the G-N_3PO system where all the reaction steps have downhill profiles. This behavior is expected since the C–N site of the FeN_4G-NP=O system cannot properly adsorb an O_2 molecule as discussed before, in contrast with the C–N site of the G-N_3PO system. This weak interaction hinders the reduction step of O_2 into HO_2. We also find that the H_2O_2 formation (pathway C) has a downhill profile on the C–N site. However, the H_2O_2 dissociation into 2*OH cannot occur on the C–N site due to the weak surface–adsorbate interaction. Therefore, this indicates that even though the ORR profile on this C–N site is energetically unfavorable, the two-electron reduction mechanism to form a H_2O_2 molecule could happen on this site, in addition to the direct $4e^-$ reduction mechanism to form water through the reduction of $*HO_2$ into *O + H_2O (pathway B), if the O_2 molecule somehow can bind to the site. As we mentioned previously, these C–N and C–N–P=O sites are responsible for formation of a very small H_2O_2 yield observed in the experiment.[59] Unfortunately, the formation of this ORR side product, H_2O_2, is not very beneficial for the fuel cell system since it will slow down the total ORR kinetics and the produced H_2O_2 will cause the degradation of perfluorinated sulfonic acid (PFSA) membranes.[89–91]

The calculated U^{onset} for the ORR on the C–N site of the G-N_3PO and FeN_4G-NP=O systems is 0.27 V and −0.24 V, corresponding to η values of 0.96 V and 1.47 V, respectively. The thermodynamic RDS for the ORR on these systems is also caused by reaction (6), the $*O_2$ reduction to $*HO_2$. The C–N site of the FeN_4G-NP=O system has a very high η because of the uphill profile that already exists at U = 0 V. The high η value of the FeN_4G-NP=O system indicates that the C–N site of the system has worse ORR performance than that of the G-N_3PO system. The calculated U^{onset} for the ORR on the C–N site of the G-N_3PO and FeN_4G-NP=O systems is comparable with that on the P–C site of the P doped graphene (PG) system (0.1–0.27 V).[49] However, the RDS for the PG system originates from the hydrogenation of *OH into H_2O.

3.3.2 Dissociative mechanism. In this section we discuss the dissociative mechanism on the FeN_4 site of the FeN_4G and FeN_4G-NP=O systems. The dissociative mechanism on the C–N site is not considered due to its weak interaction with O_2 molecules.

A very high activation energy is expected for the O_2 dissociation on this C–N site.

For the case of the FeN_4 site, the O_2 dissociation begins from the O_2 end-on adsorption state. The surface unbound O atom of the adsorbed O_2 molecule attacks the nearest C–C bond during the dissociation process. This dissociation results in an Fe–O bond at the FeN_4 site and C–O bonds at the C–C networks as shown in Fig. S11 of the ESI.† The activation energies for O_2 dissociation on the FeN_4 site of the FeN_4G and FeN_4G-NP=O systems are about 1.05 eV and 1.01 eV, respectively. These values are comparable with a previous DFT calculation by Orellana for O_2 dissociation on the FeN_4G system (1.10 eV).[13]

Starting from the 2*O configuration, there are two possibilities for the subsequent reduction reactions. The reaction either starts from the reduction of *O on the Fe site or from *O on the C site. The dissociative mechanisms on the FeN_4 site of the FeN_4G and FeN_4G-NP=O systems are composed of the following reactions:

$$* + O_{2(g)} \rightarrow *O_2 \quad (10)$$

$$*O_2 \rightarrow *O^{[Fe]} + *O^{[C]} \quad (11)$$

$$*O^{[Fe]} + *O^{[C]} + H^+ + e^-(U) \rightarrow *OH^{[Fe]} + *O^{[C]} \quad (12a)$$

$$*O^{[Fe]} + *O^{[C]} + H^+ + e^-(U) \rightarrow *O^{[Fe]} + *OH^{[C]} \quad (12b)$$

$$*OH^{[Fe]} + *O^{[C]} + H^+ + e^-(U) \rightarrow *O^{[C]} + H_2O_{(l)} \quad (13a)$$

$$*O^{[Fe]} + *OH^{[C]} + H^+ + e^-(U) \rightarrow *O^{[Fe]} + H_2O_{(l)} \quad (13b)$$

$$*O^{[C]} + H^+ + e^-(U) \rightarrow *OH^{[C]} \quad (14a)$$

$$*O^{[Fe]} + H^+ + e^-(U) \rightarrow *OH^{[Fe]} \quad (14b)$$

$$*OH^{[C]} + H^+ + e^-(U) \rightarrow H_2O_{(l)} + *, \quad (15a)$$

$$*OH^{[Fe]} + H^+ + e^-(U) \rightarrow H_2O_{(l)} + *, \quad (15b)$$

where $*X^{[Y]}$ represents an adsorbed X species on the Y site.

These reactions consist of two main branches:

D (10) → (11) → (12a) → (13a) → (14a) → (15a)

E (10) → (11) → (12b) → (13b) → (14b) → (15b)

These reaction pathways only differ in the order of the reduction sites. The calculated ORR profiles for the dissociative mechanisms on the FeN_4 site at U = 0 V through paths D and E are shown in Fig. 7. The ORR profiles at equilibrium potential U = 1.23 V are presented in Section S4 of the ESI.†

We find that all of the reduction steps have downhill profiles at U = 0 V. The ORR profiles for both of the FeN_4G and FeN_4G-NP=O systems are also quite similar, except for the second *O reduction step on the C site (reaction (14a)). Reaction (14a) on the FeN_4G-NP=O system is more exothermic than that on the FeN_4G system. This is because the *OH adsorption state on the C–C networks of the FeN_4G-NP=O system is much more stable than that of the FeN_4G system. In contrast to the undoped FeN_4G system, the co-existence of the neighboring FeN_4 and P=O sites in the FeN_4G-NP=O system perturbs the local planarity of the surrounding C–C networks. The distortion of the C–C networks facilitates the C atoms to interact with the adsorbate and this interaction will result in a relatively more stable adsorption state as compared to the adsorption on the undoped FeN_4G system. The adsorption configuration of OH on this C site is shown in Fig. S12 of the ESI.† A similar mechanism also occurs in the interaction between the neighboring quaternary-N (C–N–C) and FeN_4 sites at the zigzag edge of graphene.[40] The distortion caused by this interaction also stabilizes the *OH adsorption state on the C atom of the C–N–C site.

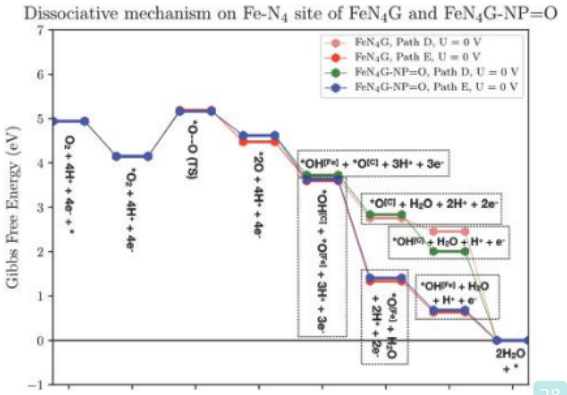

Fig. 7 ORR energy profiles for the dissociative mechanism on the FeN_4 site of the FeN_4G-NP=O system compared to that of the undoped FeN_4G system.

The calculated U^{onset} and η for the dissociative mechanism through the two reaction pathways on the FeN_4G and FeN_4G-NP=O systems are tabulated in Table 3. We find that these pathways have different η and thermodynamic RDSs, unlike the case of the associative mechanism where all pathways share the same RDS. This is because the inclusion of O_2 dissociation bypasses the HO_2 formation step, which is the common RDS for the associative mechanism on the FeN_4 site. The RDSs for the dissociative mechanisms are shifted to reactions (14a) and (15b) for pathways D and E, respectively.

We find that the difference in η for pathway E on the FeN_4G-NP=O and FeN_4G systems is modest, on the order of ~0.05 V. This is because the RDS of this pathway is the reduction of *OH into water on the FeN_4 site, which has similar ΔG values for both systems. This reduction step is identical to reaction (9) of the associative mechanism (see Fig. 5). The more profound difference is found in pathway D. η for pathway D on the FeN_4G-NP=O system is much lower than that on the FeN_4G system. The RDS for this pathway is the reduction of *O into *OH on the C site. The value of ΔG for this step is again related to the *OH adsorption strength on the C site of the system. The stabilization of the *OH adsorption state on the FeN_4G-NP=O system makes this system have a much better η value.

3.4 Discussion

The results from this study can be used to explain the ORR activity trend found in the experiment by Hu *et al.*[59] First, they find that the P doped pyrolyzed Fe/N/C catalyst has a similar onset potential to the standard pyrolyzed Fe/N/C catalyst. Our

calculation result on the associative mechanism on the FeN_4 site of the FeN_4G-NP=O system is in agreement with their finding. We find that the presence of the P=O site does not disturb the electronic structure of the FeN_4 site. It causes the ORR profile for the associative mechanism on the FeN_4 site of the FeN_4G-NP=O system to become similar to that of the undoped FeN_4G system and hence results in a quite similar onset potential. Since the FeN_4G configuration is known as the active site of the typical pyrolyzed Fe/N/C catalyst, this finding explains why the P doped Fe/N/C catalyst has a similar onset potential to the undoped one. Second, they find that the P doped pyrolyzed Fe/N/C catalyst has much higher current densities than the standard pyrolyzed Fe/N/C catalyst. This improvement is attributed to the increase in the active site density of the catalyst through the formation of various metal free sites such as C–N, C–P, and C–P–N active sites in addition to the FeN_x active sites.[59] Our calculations show that these metal free sites could catalyze the ORR quite well, although some of them prefer to produce peroxide instead of water. Another contributing factor is the activation of the ORR dissociation pathway on the FeN_4 site of the FeN_4G-NP=O system. Although this pathway is slightly hindered by the O_2 dissociation step, the positive interaction between the FeN_4 and the P=O sites improves the ORR profile for the pathway quite significantly as compared to the undoped FeN_4G system. This interaction makes both the associative and dissociative pathways become viable, hence improving the flexibility of the FeN_4 site towards the ORR. These mentioned factors allow the catalyst to produce a better current profile than the standard pyrolyzed Fe/N/C catalyst.

From our computational results, we can also extract important insights that can be used as a new strategy to improve the ORR profile of the neighboring TM–N_4 and metal-free active sites of the pyrolyzed TM/N/C-based catalyst. These insights can be obtained from the ORR profile of the FeN_4G-NP=O system through the dissociation mechanism. We find a significant improvement in the η value since the RDS for this pathway involves the reduction of *O into *OH on the C atom next to the FeN_4 site. Unlike the case of the FeN_4 site, the ΔG profile for this step on the C site of the FeN_4G-NP=O system differs significantly from that of the undoped FeN_4G system. The value of ΔG for this step on the FeN_4G-NP=O system is more exothermic due to the significant stabilization of the *OH adsorption state on the C atom, which is induced by distortion of the local planarity of the C–C networks around the neighboring FeN_4 and P=O sites as discussed before. This finding suggests that the ORR profiles of the O_2 dissociative mechanism, which involves a TM–N_4 and a C–C site, might be improved if the local planarity of the C–C networks is distorted. Various type of defects such as point defects or substitutional defects are able to distort the planarity of a graphene system.[50,55,92–98] Such defects might also be introduced near the TM–N_4 site to distort the local planarity of the C–C networks of the TM–N_4G system since this system also exhibits a graphitic structure. In addition to this mechanism, we also need to consider the activation energy for O_2 dissociation on the TM–N_4 site. Even though the dissociation mechanism gives a low η for the FeN_4G-NP=O system, it is slightly difficult for this mechanism to occur since it requires a moderate O_2 dissociation energy to initiate the reaction. The ORR through the dissociation mechanism will be more feasible if we can reduce the activation energy for O_2 dissociation. This requirement might be achieved by changing the transition metal type,[13,14,19,86] or by using other TM–N_x configurations.[18,42,73] Therefore, the ORR profile *via* the dissociation mechanism might be improved by combining the following conditions: (1) lowering the O_2 dissociation energy through the modification of the TM–N_x structure and (2) stabilizing the *OH adsorption state by distorting the local planarity of the C–C networks around the TM–N_x site.

4 Summary

The ORR mechanism on the active sites of a P-doped pyrolyzed Fe/N/C catalyst has been studied by using density functional theory based calculations. The FeN_4 site forms a direct bond with the P_{subs} and N_{subs} sites in the most stable active site configuration. Initially there are three possible active sites for this system, which are the FeN_4, C–N and P_{subs} sites. Interaction of the P_{subs} site with an O_2 molecule modifies the site into an inherently stable P=O configuration, which is less active toward O_2 molecules. Moreover, due to the formation of direct bonding between N_{subs} and P_{subs} sites, the surrounding C–N sites become discouraged to interact properly with the incoming O_2 molecule. Even so, the FeN_4 site is still able to effectively reduce O_2 molecules into water on this system.

We find that the presence of neighboring metal-free active sites does not significantly alter the electronic structure of the FeN_4 site of the FeN_4G-NP=O system. Due to this observation, the properties of atomic or molecular adsorption on the FeN_4 site of this system become similar to that on the undoped FeN_4G system. The same situation also occurs in the ORR profiles for the associative mechanism since all of the involved reactions proceed on top of the Fe atom of the FeN_4 configuration. In contrast, the dissociative mechanism produces different ORR profiles since this reduction mechanism involves both the FeN_4 site and the neighboring C–C networks. The presence of the neighboring FeN_4 and P=O sites in the FeN_4G-NP=O system distorts the local planarity of the C–C networks around them and this distortion stabilizes the *OH adsorption state on the C site. Such stabilization contributes to a significant improvement in the ORR profiles for the dissociative mechanism, even though this mechanism still requires a high activation energy for the O_2 dissociation step.

Using the insights obtained from our results, we also proposed a new strategy to make the ORR dissociation mechanism become more feasible on the active sites of pyrolyzed TM/N/C catalysts. The ORR profile *via* the dissociation mechanism might be improved by combining the following conditions: (1) lowering the O_2 dissociation energy through the modification of the TM–N_x structure and (2) stabilizing the *OH adsorption state on the C site by distorting the local planarity of the C–C networks around the TM–N_x site through substitutional doping or point defects.

Conflicts of interest

There are no conflicts to declare.

Acknowledgements

This work is supported by the Directorate of Higher Education, Ministry of Research Technology and Higher Education (RISTEKDIKTI), Republic of Indonesia under grant scheme "Penelitian Dasar Unggulan Perguruan Tinggi 2018". HKD and MKA appreciate support from RISTEKDIKTI through the "World Class Professor" program. All calculations were performed using the High Performance Computer facility at the Research Center for Nanosciences and Nanotechnology, Institut Teknologi Bandung.

Notes and references

1 M. Shao, Q. Chang, J.-P. Dodelet and R. Chenitz, *Chem. Rev.*, 2016, **116**, 3594–3657.
2 A. A. Gewirth, J. A. Varnell and A. M. DiAscro, *Chem. Rev.*, 2018, **118**, 2313–2339.
3 F. Jaouen, E. Proietti, M. Lefevre, R. Chenitz, J.-P. Dodelet, G. Wu, H. T. Chung, C. M. Johnston and P. Zelenay, *Energy Environ. Sci.*, 2011, **4**, 114–130.
4 G. Wu, K. L. More, C. M. Johnston and P. Zelenay, *Science*, 2011, **332**, 443–447.
5 M. Lefèvre, E. Proietti, F. Jaouen and J.-P. Dodelet, *Science*, 2009, **324**, 71–74.
6 Z. Chen, D. Higgins, A. Yu, L. Zhang and J. Zhang, *Energy Environ. Sci.*, 2011, **4**, 3167–3192.
7 C. Medard, M. Lefévre, J. Dodelet, F. Jaouen and G. Lindbergh, *Electrochim. Acta*, 2006, **51**, 3202–3213.
8 J. M. Ziegelbauer, T. S. Olson, S. Pylypenko, F. Alamgir, C. Jaye, P. Atanassov and S. Mukerjee, *J. Phys. Chem. C*, 2008, **112**, 8839–8849.
9 Q. Jia, N. Ramaswamy, U. Tylus, K. Strickland, J. Li, A. Serov, K. Artyushkova, P. Atanassov, J. Anibal, C. Gumeci, S. C. Barton, M.-T. Sougrati, F. Jaouen, B. Halevi and S. Mukerjee, *Nano Energy*, 2016, **29**, 65–82.
10 D. Guo, R. Shibuya, C. Akiba, S. Saji, T. Kondo and J. Nakamura, *Science*, 2016, **351**, 361–365.
11 W. Liu, L. Zhang, X. Liu, X. Liu, X. Yang, S. Miao, W. Wang, A. Wang and T. Zhang, *J. Am. Chem. Soc.*, 2017, **139**, 10790–10798.
12 D. H. Lee, W. J. Lee, W. J. Lee, S. O. Kim and Y.-H. Kim, *Phys. Rev. Lett.*, 2011, **106**, 175502.
13 W. Orellana, *J. Phys. Chem. C*, 2013, **117**, 9812–9818.
14 F. Calle-Vallejo, J. I. Martinez and J. Rossmeisl, *Phys. Chem. Chem. Phys.*, 2011, **13**, 15639–15643.
15 H. K. Dipojono, A. G. Saputro, R. Belkada, H. Nakanishi, H. Kasai, M. David and E. Sy Dy, *J. Phys. Soc. Jpn.*, 2009, **78**, 094710.
16 H. K. Dipojono, A. G. Saputro, S. M. Aspera and H. Kasai, *Jpn. J. Appl. Phys.*, 2011, **50**, 055702.
17 A. G. Saputro, F. Rusydi, H. Kasai and H. K. Dipojono, *J. Phys. Soc. Jpn.*, 2012, **81**, 034703.
18 A. G. Saputro and H. Kasai, *J. Phys. Soc. Jpn.*, 2014, **83**, 024707.
19 A. G. Saputro, H. Kasai, K. Asazawa, H. Kishi and H. Tanaka, *J. Phys. Soc. Jpn.*, 2013, **82**, 114704.
20 S. Kattel, P. Atanassov and B. Kiefer, *Phys. Chem. Chem. Phys.*, 2013, **15**, 148–153.
21 S. Kattel, P. Atanassov and B. Kiefer, *J. Phys. Chem. C*, 2012, **116**, 17378–17383.
22 S. Kattel and G. Wang, *J. Phys. Chem. Lett.*, 2014, **5**, 452–456.
23 S. Kattel, P. Atanassov and B. Kiefer, *Phys. Chem. Chem. Phys.*, 2014, **16**, 13800–13806.
24 S. Kattel and G. Wang, *J. Mater. Chem. A*, 2013, **1**, 10790–10797.
25 F. Rusydi, M. K. Agusta, A. G. Saputro and H. Kasai, *J. Phys. Soc. Jpn.*, 2012, **81**, 124301.
26 T. Ikeda, M. Boero, S.-F. Huang, K. Terakura, M. Oshima and J.-I. Ozaki, *J. Phys. Chem. C*, 2008, **112**, 14706–14709.
27 X. Wang, Z. Hou, T. Ikeda, S.-F. Huang, K. Terakura, M. Boero, M. Oshima, M.-A. Kakimoto and S. Miyata, *Phys. Rev. B: Condens. Matter Mater. Phys.*, 2011, **84**, 245434.
28 X. Bao, X. Nie, D. Deak, E. Biddinger, W. Luo, A. Asthagiri, U. Ozkan and C. Hadad, *Top. Catal.*, 2013, **56**, 1623–1633.
29 H. Kim, K. Lee, S. I. Woo and Y. Jung, *Phys. Chem. Chem. Phys.*, 2011, **13**, 17505–17510.
30 F. Studt, *Catal. Lett.*, 2013, **143**, 58–60.
31 J. Dai and J. Yuan, *Phys. Rev. B: Condens. Matter Mater. Phys.*, 2010, **81**, 165414.
32 J. Zhang, Z. Wang and Z. Zhu, *J. Mol. Model.*, 2013, **19**, 5515–5521.
33 M. Li, L. Zhang, Q. Xu, J. Niu and Z. Xia, *J. Catal.*, 2014, **314**, 66–72.
34 L. Zhang and Z. Xia, *J. Phys. Chem. C*, 2011, **115**, 11170–11176.
35 K. A. Kurak and A. B. Anderson, *J. Phys. Chem. C*, 2009, **113**, 6730–6734.
36 R. A. Sidik, A. B. Anderson, N. P. Subramanian, S. P. Kumaraguru and B. N. Popov, *J. Phys. Chem. B*, 2006, **110**, 1787–1793.
37 E. Vayner and A. B. Anderson, *J. Phys. Chem. C*, 2007, **111**, 9330–9336.
38 M. Jain, S.-h. Chou and A. Siedle, *J. Phys. Chem. B*, 2006, **110**, 4179–4185.
39 L. Qin, L. Wang, X. Yang, R. Ding, Z. Zheng, X. Chen and B. Lv, *J. Catal.*, 2018, **359**, 242–250.
40 A. G. Saputro and H. Kasai, *Phys. Chem. Chem. Phys.*, 2015, **17**, 3059–3071.
41 A. K. Fajrial, A. G. Saputro, M. K. Agusta, F. Rusydi, Nugraha and H. K. Dipojono, *Phys. Chem. Chem. Phys.*, 2017, **19**, 23497–23504.
42 E. F. Holby, G. Wu, P. Zelenay and C. D. Taylor, *J. Phys. Chem. C*, 2014, **118**, 14388–14393.
43 G. Zhao, L. Shi, J. Xu, X. Yan and T. Zhao, *Int. J. Hydrogen Energy*, 2018, **43**, 1470–1478.
44 M. D. Esrafili and P. Mousavian, *Appl. Surf. Sci.*, 2018, **440**, 580–585.
45 N. Yang, X. Zheng, L. Li, J. Li and Z. Wei, *J. Phys. Chem. C*, 2017, **121**, 19321–19328.
46 M. D. Bhatt, G. Lee and J. S. Lee, *J. Phys. Chem. C*, 2016, **120**, 26435–26441.

47 E. Gracia-Espino, *J. Phys. Chem. C*, 2016, **120**, 27849–27857.
48 F. He, K. Li, G. Xie, Y. Wang, M. Jiao, H. Tang and Z. Wu, *Phys. Chem. Chem. Phys.*, 2016, **18**, 12675–12681.
49 X. Bai, E. Zhao, K. Li, Y. Wang, M. Jiao, F. He, X. Sun, H. Sun and Z. Wu, *Carbon*, 2016, **105**, 214–223.
50 X. Zhang, Z. Lu, Z. Fu, Y. Tang, D. Ma and Z. Yang, *J. Power Sources*, 2015, **276**, 222–229.
51 R. Li, Z. Wei and X. Gou, *ACS Catal.*, 2015, **5**, 4133–4142.
52 U. B. Nasini, V. Gopal Bairi, S. Kumar Ramasahayam, S. E. Bourdo, T. Viswanathan and A. U. Shaikh, *ChemElectroChem*, 2014, **1**, 573–579.
53 H. Jiang, Y. Zhu, Q. Feng, Y. Su, X. Yang and C. Li, *Chem. – Eur. J.*, 2014, **20**, 3106–3112.
54 J. P. Paraknowitsch, Y. Zhang, B. Wienert and A. Thomas, *Chem. Commun.*, 2013, **49**, 1208–1210.
55 M. Kaukonen, A. Krasheninnikov, E. Kauppinen and R. Nieminen, *ACS Catal.*, 2013, **3**, 159–165.
56 C. H. Choi, S. H. Park and S. I. Woo, *J. Mater. Chem.*, 2012, **22**, 12107–12115.
57 C. H. Choi, S. H. Park and S. I. Woo, *ACS Nano*, 2012, **6**, 7084–7091.
58 D. Yu, Y. Xue and L. Dai, *J. Phys. Chem. Lett.*, 2012, **3**, 2863–2870.
59 Y. Hu, J. Zhu, Q. Lv, C. Liu, Q. Li and W. Xing, *Electrochim. Acta*, 2015, **155**, 335–340.
60 X.-D. Yang, Y. Zheng, J. Yang, W. Shi, J.-H. Zhong, C. Zhang, X. Zhang, Y.-H. Hong, X.-X. Peng, Z.-Y. Zhou and S.-G. Sun, *ACS Catal.*, 2017, **7**, 139–145.
61 A. Zitolo, V. Goellner, V. Armel, M.-T. Sougrati, T. Mineva, L. Stievano, E. Fonda and F. Jaouen, *Nat. Mater.*, 2015, **14**, 937–942.
62 U. I. Kramm, I. Herrmann-Geppert, J. Behrends, K. Lips, S. Fiechter and P. Bogdanoff, *J. Am. Chem. Soc.*, 2016, **138**, 635–640.
63 A. K. Fajrial, M. F. Abdulkarim, A. G. Saputro, M. K. Agusta and H. K. Dipojono, *Procedia Eng.*, 2017, **170**, 131–135.
64 P. Hohenberg and W. Kohn, *Phys. Rev.*, 1964, **136**, B864–B871.
65 W. Kohn and L. J. Sham, *Phys. Rev.*, 1965, **140**, A1133–A1138.
66 P. Giannozzi, S. Baroni, N. Bonini, M. Calandra, R. Car, C. Cavazzoni, D. Ceresoli, G. L. Chiarotti, M. Cococcioni, I. Dabo, A. D. Corso, S. de Gironcoli, S. Fabris, G. Fratesi, R. Gebauer, U. Gerstmann, C. Gougoussis, A. Kokalj, M. Lazzeri, L. Martin-Samos, N. Marzari, F. Mauri, R. Mazzarello, S. Paolini, A. Pasquarello, L. Paulatto, C. Sbraccia, S. Scandolo, G. Sclauzero, A. P. Seitsonen, A. Smogunov, P. Umari and R. M. Wentzcovitch, *J. Phys.: Condens. Matter*, 2009, **21**, 395502.
67 J. P. Perdew, K. Burke and M. Ernzerhof, *Phys. Rev. Lett.*, 1996, **77**, 3865–3868.
68 D. Vanderbilt, *Phys. Rev. B: Condens. Matter Mater. Phys.*, 1990, **41**, 7892–7895.
69 S. Grimme, *J. Comput. Chem.*, 2006, **27**, 1787–1799.
70 S. R. Bahn and K. W. Jacobsen, *Comput. Sci. Eng.*, 2002, **4**, 56–66.
71 G. Henkelman, B. P. Uberuaga and H. Jansson, *J. Chem. Phys.*, 2000, **113**, 9901–9904.
72 J. K. Nörskov, J. Rossmeisl, A. Logadottir, L. Lindqvist, J. R. Kitchin, T. Bligaard and H. Jònsson, *J. Phys. Chem. B*, 2004, **108**, 17886–17892.
73 C. E. Szakacs, M. Lefevre, U. I. Kramm, J.-P. Dodelet and F. Vidal, *Phys. Chem. Chem. Phys.*, 2014, **16**, 13654–13661.
74 W.-J. Jiang, L. Gu, L. Li, Y. Zhang, X. Zhang, L.-J. Zhang, J.-Q. Wang, J.-S. Hu, Z. Wei and L.-J. Wan, *J. Am. Chem. Soc.*, 2016, **138**, 3570–3578.
75 B. Zheng, J. Wang, F.-B. Wang and X.-H. Xia, *Electrochem. Commun.*, 2013, **28**, 24–26.
76 J. Tai, J. Hu, Z. Chen and H. Lu, *RSC Adv.*, 2014, **4**, 61437–61443.
77 L. Qu, Y. Liu, J.-B. Baek and L. Dai, *ACS Nano*, 2010, **4**, 1321–1326.
78 N. D. M. Hine, K. Frensch, W. M. C. Foulkes and M. W. Finnis, *Phys. Rev. B: Condens. Matter Mater. Phys.*, 2009, **79**, 024112.
79 S. Kirklin, J. E. Saal, B. Meredig, A. Thompson, J. W. Doak, M. Aykol, S. Ruhl and C. Wolverton, *npj Comput. Mater.*, 2015, **1**, 15010.
80 S. Gupta, S. Zhao, O. Ogoke, Y. Lin, H. Xu and G. Wu, *ChemSusChem*, 2017, **10**, 774–785.
81 R. Hultgren, N. Gingrich and B. Warren, *J. Chem. Phys.*, 1935, **3**, 351–355.
82 R. Wyckoff, *Crystal structures, rocksalt structure*, Interscience Publishers, New York, 1963, pp. 85–237.
83 L. Cartz, S. Srinivasa, R. Riedner, J. Jorgensen and T. Worlton, *J. Chem. Phys.*, 1979, **71**, 1718–1721.
84 S. Li, W. Xu, P. Cheng, J. Luo, D. Zhou, J. Li, R. Li and D. Yuan, *Synth. Met.*, 2017, **223**, 137–144.
85 M. Tsuda, W. A. Dino, H. Nakanishi and H. Kasai, *Chem. Phys. Lett.*, 2005, **402**, 71–74.
86 M. Tsuda, E. Sy Dy and H. Kasai, *J. Chem. Phys.*, 2005, **122**, 244719.
87 T. Q. Nguyen, M. C. S. Escaño, N. Shimoji, H. Nakanishi and H. Kasai, *Phys. Rev. B: Condens. Matter Mater. Phys.*, 2008, **77**, 1–7.
88 W. Liang, J. Chen, Y. Liu and S. Chen, *ACS Catal.*, 2014, **4**, 4170–4177.
89 M. Aoki, H. Uchida and M. Watanabe, *Electrochem. Commun.*, 2006, **8**, 1509–1513.
90 J. Qiao, M. Saito, K. Hayamizu and T. Okada, *J. Electrochem. Soc.*, 2006, **153**, A967–A974.
91 D. E. Curtin, R. D. Lousenberg, T. J. Henry, P. C. Tangeman and M. E. Tisack, *J. Power Sources*, 2004, **131**, 41–48.
92 A. G. Saputro, A. K. Fajrial, M. K. Agusta and H. K. Dipojono, *J. Phys.: Conf. Ser.*, 2019, **1204**, 012119.
93 F. Mehmood, R. Pachter, W. Lu and J. J. Boeckl, *J. Phys. Chem. C*, 2013, **117**, 10366–10374.
94 Z. Lu, S. Li, C. Liu, C. He, X. Yang, D. Ma, G. Xu and Z. Yang, *RSC Adv.*, 2017, **7**, 20398–20405.
95 Z. Ao, J. Yang, S. Li and Q. Jiang, *Chem. Phys. Lett.*, 2008, **461**, 276–279.
96 M. Chi and Y.-P. Zhao, *Comput. Mater. Sci.*, 2009, **46**, 1085–1090.
97 Y. Chen, B. Gao, J.-X. Zhao, Q.-H. Cai and H.-G. Fu, *J. Mol. Model.*, 2012, **18**, 2043–2054.
98 Y. Chen, X.-c. Yang, Y.-j. Liu, J.-x. Zhao, Q.-h. Cai and X.-z. Wang, *J. Mol. Graphics Modell.*, 2013, **39**, 126–132.

Oxygen reduction reaction mechanism on a phosporus-doped pyrolyzed graphitic Fe/N/C catalyst

ORIGINALITY REPORT

20%	11%	19%	4%
SIMILARITY INDEX	INTERNET SOURCES	PUBLICATIONS	STUDENT PAPERS

PRIMARY SOURCES

1	Li, W.. "Kinetics and mechanism of pyruvic acid degradation by ozone in the presence of PdO/CeO"2", Applied Catalysis B, Environmental, 20120222 Publication	1%
2	Koichiro Asazawa, Hirofumi Kishi, Hirohisa Tanaka, Daiju Matsumura et al. "In Situ XAFS and HAXPES Analysis and Theoretical Study of Cobalt Polypyrrole Incorporated on Carbon (CoPPyC) Oxygen Reduction Reaction Catalysts for Anion-Exchange Membrane Fuel Cells", The Journal of Physical Chemistry C, 2014 Publication	1%
3	Adhitya Gandaryus Saputro, Apresio Kefin Fajrial, Mohammad Kemal Agusta, Hermawan Kresno Dipojono. "Density Functional Study on the Formation of Sulfur-doped Configuration on the Active Site of Pyrolyzed Fe/N/C Catalyst", Journal of Physics: Conference Series, 2019	1%

	Publication	
4	Elham Ashori, Fariba Nazari, Francesc Illas. " Influence of NO and (NO) adsorption on the properties of Fe-N4 porphyrin-like graphene sheets ", Physical Chemistry Chemical Physics, 2017 Publication	1 %
5	journals.jps.jp Internet Source	1 %
6	Submitted to School of Business and Management ITB Student Paper	1 %
7	Nugraha, Adhitya Gandaryus Saputro, Mohammad Kemal Agusta, Brian Yuliarto, Hermawan K. Dipojono, Febdian Rusydi, Ryo Maezono. "Selectivity of CO and NO adsorption on ZnO (0002) surfaces: A DFT investigation", Applied Surface Science, 2017 Publication	1 %
8	eprints.itb.ac.id Internet Source	1 %
9	aip.scitation.org Internet Source	<1 %
10	repository.wima.ac.id Internet Source	<1 %
11	chemistry-europe.onlinelibrary.wiley.com Internet Source	

<1 %

12 Adhitya Gandaryus Saputro, Arifin Luthfi Maulana, Fadjar Fathurrahman, Ganes Shukri et al. "Density functional and microkinetic study of CO2 hydrogenation to methanol on subnanometer Pd cluster doped by transition metal (M= Cu, Ni, Pt, Rh)", International Journal of Hydrogen Energy, 2021 <1 %
Publication

13 Walter Orellana. " Catalytic Properties of Transition Metal–N Moieties in Graphene for the Oxygen Reduction Reaction: Evidence of Spin-Dependent Mechanisms ", The Journal of Physical Chemistry C, 2013 <1 %
Publication

14 onlinelibrary.wiley.com <1 %
Internet Source

15 Dongwei Ma, Zhi Wang, Haitao Cui, Jun Zeng, Chaozheng He, Zhansheng Lu. "First-principles study of O2 adsorption on Al-doped ZnO(1 0 1¯ 0) surface", Sensors and Actuators B: Chemical, 2016 <1 %
Publication

16 Anton V. Kuzmin, Bagrat A. Shainyan. " Theoretical Density Functional Theory Study of Electrocatalytic Activity of MN -Doped (M = <1 %

Cu, Ag, and Zn) Single-Walled Carbon Nanotubes in Oxygen Reduction Reactions ", ACS Omega, 2020
Publication

---

17 Alfred B. Anderson, Edward F. Holby. " Pathways for O Electroreduction over Substitutional FeN , HOFeN , and OFeN in Graphene Bulk Sites: Critical Evaluation of Overpotential Predictions Using LGER and CHE Models ", The Journal of Physical Chemistry C, 2019 <1 %
Publication

---

18 etheses.whiterose.ac.uk <1 %
Internet Source

---

19 Apresio Kefin Fajrial, Muhammad Fadhil Abdulkarim, Adhitya Gandaryus Saputro, Mohammad Kemal Agusta et al. "Boron and Nitrogen Co-doping Configuration on Pyrolyzed Fe-N 4 /C Catalyst", Procedia Engineering, 2017 <1 %
Publication

---

20 Liyan Feng, Yuejie Liu, Jingxiang Zhao. " Fe– and Co–P -embedded graphenes as electrocatalysts for the oxygen reduction reaction: theoretical insights ", Physical Chemistry Chemical Physics, 2015 <1 %
Publication

21	Yang Hu, Jianbin Zhu, Qing Lv, Changpeng Liu, Qingfeng Li, Wei Xing. "Promotional effect of phosphorus doping on the activity of the Fe-N/C catalyst for the oxygen reduction reaction", Electrochimica Acta, 2015 Publication	<1 %
22	Adhitya G. Saputro, Febdian Rusydi, Hideaki Kasai, Hermawan K. Dipojono. "Oxygen Reduction Reaction on Cobalt–(6)Pyrrole Cluster: Density Functional Theory Study", Journal of the Physical Society of Japan, 2012 Publication	<1 %
23	Adhitya G. Saputro, Hideaki Kasai. " Density Functional Theory Study on the Interaction of O and H O Molecules with the Active Sites of Cobalt–Polypyrrole Catalyst ", Journal of the Physical Society of Japan, 2014 Publication	<1 %
24	Arifin Luthfi Maulana, Refaldi Intri Dwi Putra, Adhitya Gandaryus Saputro, Mohammad Kemal Agusta et al. " DFT and microkinetic investigation of methanol synthesis CO hydrogenation on Ni(111)-based surfaces ", Physical Chemistry Chemical Physics, 2019 Publication	<1 %
25	Ni Luh Wulan Septiani, Adhitya Gandaryus Saputro, Yusuf Valentino Kaneti, Arifin Luthfi Maulana et al. "Hollow Zinc Oxide	<1 %

Microsphere-Multiwalled Carbon Nanotubes Composites for Selective Detection of Sulfur Dioxide", ACS Applied Nano Materials, 2020
Publication

26	coek.info Internet Source	<1%
27	Ruixuan Qin, Pengxin Liu, Gang Fu, Nanfeng Zheng. "Strategies for Stabilizing Atomically Dispersed Metal Catalysts", Small Methods, 2018 Publication	<1%
28	Jiali Gao, Chunyan Guo, Xin Wang, Wenxu Zhang, Yang Wang, Vahid Vahabi. "Porphyrin-like porous nanomaterials as drug delivery systems for ibuprofen drug", Molecular Physics, 2019 Publication	<1%
29	notendur.hi.is Internet Source	<1%
30	Bombi, G.G.. "2-Hydroxy-3-carboxy-dihydrocinnamic acid: Complexation properties towards aluminium(III) and iron(III)", Polyhedron, 20070806 Publication	<1%
31	Bai, Xiaowan, Erjun Zhao, Kai Li, Ying Wang, Menggai Jiao, Feng He, Xiaoxu Sun, He Sun, and Zhijian Wu. "Theoretical insights on the	<1%

reaction pathways for oxygen reduction reaction on phosphorus doped graphene", Carbon, 2016.
Publication

---

32 Jiayi Xu, Ayyappan Elangovan, Jun Li, Bin Liu. "Graphene-Based Dual-Metal Sites for Oxygen Reduction Reaction: A Theoretical Study", The Journal of Physical Chemistry C, 2021 <1 %
Publication

---

33 "Non-Noble Metal Fuel Cell Catalysts", Wiley, 2014 <1 %
Publication

---

34 Ohnishi, R.. "Niobium-based catalysts prepared by reactive radio-frequency magnetron sputtering and arc plasma methods as non-noble metal cathode catalysts for polymer electrolyte fuel cells", Electrochimica Acta, 20100730 <1 %
Publication

---

35 Shyam Kattel, Guofeng Wang. "A density functional theory study of oxygen reduction reaction on Me–N4 (Me = Fe, Co, or Ni) clusters between graphitic pores", Journal of Materials Chemistry A, 2013 <1 %
Publication

---

36 Xiaoming Zhang, Shansheng Yu, Hong Chen, Weitao Zheng. "TM atoms on B/N doped defective graphene as a catalyst for oxygen <1 %

reduction reaction: a theoretical study", RSC Advances, 2015
Publication

37	docplayer.net Internet Source	<1%
38	Yongcheng Li, Riming Hu, Xin Wan, Jia‐Xiang Shang, Fu‐He Wang, Jianglan Shui. "Density Functional Theory Calculation of Zn and N Codoped Graphene for Oxygen Reduction and Evolution Reactions", Advanced Theory and Simulations, 2020 Publication	<1%
39	Geng, Dongsheng, Ning Ding, T. S. Andy Hor, Zhaolin Liu, Xueliang Sun, and Yun Zong. "Potential of metal-free “graphene alloy” as electrocatalysts for oxygen reduction reaction", Journal of Materials Chemistry A, 2014. Publication	<1%
40	Kiranpal Singh, Fatemeh Razmjooei, Jong-Sung Yu. "Active sites and factors influencing them for efficient oxygen reduction reaction in metal-N coordinated pyrolyzed and non-pyrolyzed catalysts: a review", Journal of Materials Chemistry A, 2017 Publication	<1%
41	Maruyama, J.. "Use of purine and pyrimidine bases as nitrogen sources of active site in	<1%

oxygen reduction catalyst", Journal of Power Sources, 20091201
Publication

---

42 Tao Sun, Yufei Jiang, Qiang Wu, Lingyu Du, Zhiqi Zhang, Lijun Yang, Xizhang Wang, Zheng Hu. "Is iron nitride or carbide highly active for oxygen reduction reaction in acidic medium?", Catalysis Science & Technology, 2017 <1 %
Publication

---

43 depositonce.tu-berlin.de <1 %
Internet Source

---

44 Ferrighi, Lara, Mario Italo Trioni, and Cristiana Di Valentin. "Boron, Nitrogen Doped and Co-Doped Graphene on Cu (111): a DFT+vdW Study", The Journal of Physical Chemistry C <1 %
Publication

---

45 Guangqi Zhu, Fan Liu, Yicheng Wang, Zidong Wei, Wei Wang. " Systematic exploration of N,C coordination effects on the ORR performance of Mn–N doped graphene catalysts based on DFT calculations ", Physical Chemistry Chemical Physics, 2019 <1 %
Publication

---

46 Guofeng Wang. "Density functional theory study of the adsorption of oxygen molecule on iron phthalocyanine and cobalt phthalocyanine", Molecular Simulation, 09/2008 <1 %

Publication

47	Lei, M.. "A highly ordered Fe-N-C nanoarray as a non-precious oxygen-reduction catalyst for proton exchange membrane fuel cells", Journal of Power Sources, 20110401 Publication	<1 %
48	Mohammad Kemal Agusta, Adhitya Gandaryus Saputro, Viny Veronika Tanuwijaya, Novianto Nur Hidayat, Hermawan Kresno Dipojono. "Hydrogen Adsorption on Fe-based Metal Organic Frameworks: DFT Study", Procedia Engineering, 2017 Publication	<1 %
49	Sun, Jing, Ya-Hui Fang, and Zhi-Pan Liu. "Electrocatalytic oxygen reduction kinetics on Fe-center of nitrogen-doped graphene", Physical Chemistry Chemical Physics, 2014. Publication	<1 %
50	Tao Sun, Bingbing Tian, Jiong Lu, Chenliang Su. "Recent advances in Fe (or Co)/N/C electrocatalysts for the oxygen reduction reaction in polymer electrolyte membrane fuel cells", Journal of Materials Chemistry A, 2017 Publication	<1 %
51	Xiaowan Bai, Erjun Zhao, Wencheng Wang, Ying Wang, Kai Li, Lin Lin, Jucai Yang, He Sun, Zhijian Wu. " A direct four-electron process on	<1 %

	Fe–N doped graphene for the oxygen reduction reaction: a theoretical perspective ", RSC Advances, 2017 Publication	
52	Xilin Zhang, Zhansheng Lu, Zongxian Yang. "The mechanism of oxygen reduction reaction on CoN4 embedded graphene: A combined kinetic and atomistic thermodynamic study", International Journal of Hydrogen Energy, 2016 Publication	<1 %
53	Yuyu Liu, Xiuping Yue, Kaixi Li, Jinli Qiao, David P. Wilkinson, Jiujun Zhang. "PEM fuel cell electrocatalysts based on transition metal macrocyclic compounds", Coordination Chemistry Reviews, 2016 Publication	<1 %
54	ir.library.osaka-u.ac.jp Internet Source	<1 %
55	krex.k-state.edu Internet Source	<1 %
56	oparu.uni-ulm.de Internet Source	<1 %
57	scholarworks.unist.ac.kr Internet Source	<1 %
58	www.rsc.org Internet Source	<1 %

59	Anastassakis, E M, and J D Joannopoulous. "The Physics of Semiconductors : 20th International Conference", The Physics of Semiconductors, 1990. Publication	<1 %
60	Anchalee Junkaew, Supawadee Namuangruk, Phornphimon Maitarad, Masahiro Ehara. " Silicon-coordinated nitrogen-doped graphene as a promising metal-free catalyst for N O reduction by CO: a theoretical study ", RSC Advances, 2018 Publication	<1 %
61	Fang, Z.. "Some basic matters on the heat effects at electrode-electrolyte interfaces", Thermochimica Acta, 20110320 Publication	<1 %
62	Febdian Rusydi, Nufida D. Aisyah, Rizka N. Fadilla, Hermawan K. Dipojono et al. "The transition state conformational effect on the activation energy of ethyl acetate neutral hydrolysis", Heliyon, 2019 Publication	<1 %
63	Gouri Chakraborty, In-Hyeok Park, Raghavender Medishetty, Jagadese J. Vittal. "Two-Dimensional Metal-Organic Framework Materials: Synthesis, Structures, Properties and Applications", Chemical Reviews, 2021 Publication	<1 %

64	Huiying Zhang, Yu Tian, Jingxiang Zhao, Qinghai Cai, Zhongfang Chen. "Small Dopants Make Big Differences: Enhanced Electrocatalytic Performance of MoS 2 Monolayer for Oxygen Reduction Reaction (ORR) by N– and P–Doping", Electrochimica Acta, 2017 Publication	<1 %
65	Li-yan Feng, Yue-jie Liu, Jing-xiang Zhao. "Iron-embedded boron nitride nanosheet as a promising electrocatalyst for the oxygen reduction reaction (ORR): A density functional theory (DFT) study", Journal of Power Sources, 2015 Publication	<1 %
66	Mehdi D. Esrafili, Safa Heydari. "CO Oxidation Catalyzed by a Single Ti Atom Supported on Divacancy Defective Graphene: A Dispersion-Corrected DFT Study", ChemistrySelect, 2018 Publication	<1 %
67	Pugazhenthiran, N., S. Murugesan, and S. Anandan. "High surface area Ag-TiO2 nanotubes for solar/visible-light photocatalytic degradation of ceftiofur sodium", Journal of Hazardous Materials, 2013. Publication	<1 %

68	Tien Quang Nguyen, Mary Clare Sison Escaño, Hiroshi Nakanishi, Hideaki Kasai, Hiroyoshi Maekawa, Kazuo Osumi, Kaoru Sato. "DFT+ U study on the oxygen adsorption and dissociation on CeO 2 -supported platinum cluster", Applied Surface Science, 2014 Publication	<1 %
69	Vincent Goellner, Claudio Baldizzone, Anna Schuppert, Moulay Tahar Sougrati, Karl Mayrhofer, Frédéric Jaouen. "Degradation of Fe/N/C catalysts upon high polarization in acid medium", Phys. Chem. Chem. Phys., 2014 Publication	<1 %
70	Weiyu Zhang, Xiaocheng Xu, Chenxing Zhang, Zihuan Yu, Yiming Zhou, Yawen Tang, Ping Wu, Shaojun Guo. " 3D Space-Confined Pyrolysis of Double-Network Aerogels Containing In-Fe Cyanogel and Polyaniline: A New Approach to Hierarchically Porous Carbon with Exclusive Fe-N Active Sites for Oxygen Reduction Catalysis ", Small Methods, 2017 Publication	<1 %
71	Xiao-Dong Yang, Yanping Zheng, Jing Yang, Wei Shi et al. "Modeling Fe/N/C Catalysts in Monolayer Graphene", ACS Catalysis, 2016 Publication	<1 %

72	Yu Wang, Hao Yuan, Yafei Li, Zhongfang Chen. "Two-dimensional iron-phthalocyanine (Fe-Pc) monolayer as a promising single-atom-catalyst for oxygen reduction reaction: a computational study", Nanoscale, 2015 Publication	<1 %
73	Zhang, Peng, Xiuli Hou, Jianli Mi, Yanqiong He, Lin Lin, Qing Jiang, and Mingdong Dong. "From two-dimension to one-dimension: the curvature effect of silicon-doped graphene and carbon nanotubes for oxygen reduction reaction", Physical Chemistry Chemical Physics, 2014. Publication	<1 %
74	Zhang, Qiang, Kuldeep Balram Mamtani, Deeksha Jain, Umit S. Ozkan, and Aravind R. Asthagiri. "CO Poisoning Effects on FeNC and CNx ORR Catalysts: A Combined Experimental-Computational Study", The Journal of Physical Chemistry C Publication	<1 %
75	Zhansheng Lu, Shuo Li, Chuang Liu, Chaozheng He, Xinwei Yang, Dongwei Ma, Guoliang Xu, Zongxian Yang. "Sulfur doped graphene as a promising metal-free electrocatalyst for oxygen reduction reaction: a DFT-D study", RSC Advances, 2017 Publication	<1 %

76	dr.ntu.edu.sg Internet Source	<1 %
77	eprints.lib.hokudai.ac.jp Internet Source	<1 %
78	epub.uni-bayreuth.de Internet Source	<1 %
79	jultika.oulu.fi Internet Source	<1 %
80	link.springer.com Internet Source	<1 %
81	mafiadoc.com Internet Source	<1 %
82	tuprints.ulb.tu-darmstadt.de Internet Source	<1 %
83	waseda.repo.nii.ac.jp Internet Source	<1 %
84	www.molgw.org Internet Source	<1 %
85	Adhitya G. Saputro, Hideaki Kasai, Koichiro Asazawa, Hirofumi Kishi, Hirohisa Tanaka. " Comparative Study on the Catalytic Activity of the TM–N Active Sites (TM = Mn, Fe, Co, Ni) in the Oxygen Reduction Reaction: Density Functional Theory Study ", Journal of the Physical Society of Japan, 2013	<1 %

Publication

86	F X. Chen. "Cobalt-Phosphorus Decorated Graphene as Electrocatalyst for Oxygen Reduction Reactions: A Density Functional Theory Study", International Journal of Electrochemical Science, 2021 Publication	<1 %
87	Hao Xu, Dan Wang, Peixia Yang, Anmin Liu, Ruopeng Li, Yun Li, Lihui Xiao, Xuefeng Ren, Jinqiu Zhang, Maozhong An. "Atomically dispersed M–N–C catalysts for the oxygen reduction reaction", Journal of Materials Chemistry A, 2020 Publication	<1 %
88	Rong Li, Zidong Wei, Xinglong Gou, Wei Xu. "Phosphorus-doped graphene nanosheets as efficient metal-free oxygen reduction electrocatalysts", RSC Advances, 2013 Publication	<1 %
89	Di Valentin, Cristiana, Lara Ferrighi, and Gianluca Fazio. "Theoretical Studies of Oxygen Reactivity of Free-Standing and Supported Boron-Doped Graphene", ChemSusChem, 2016. Publication	<1 %
90	Gao, Feng, Guang-Lin Zhao, Zhou Wang, Diola Bagayoko, and Di-Jia Liu. "Catalytic reaction on FeN4/C site of nitrogen functionalized	<1 %

carbon nanotubes as cathode catalyst for hydrogen fuel cells", Catalysis Communications, 2015.
Publication

91	iopscience.iop.org Internet Source	<1 %

Exclude quotes	Off	Exclude matches	Off
Exclude bibliography	On		

Oxygen reduction reaction mechanism on a phosporus-doped pyrolyzed graphitic Fe/N/C catalyst

GRADEMARK REPORT

FINAL GRADE

/0

GENERAL COMMENTS

Instructor

PAGE 1

PAGE 2

PAGE 3

PAGE 4

PAGE 5

PAGE 6

PAGE 7

PAGE 8

PAGE 9

PAGE 10

PAGE 11